RSC Advances

PAPER

View Article Online
View Journal | View Issue

Cite this: *RSC Adv.*, 2024, **14**, 23816

Optimizing methylene blue adsorption conditions on hydrothermally synthesized NaX zeolite through a full two-level factorial design†

Hammoudi Hadda Aya,[a] Nibou Djamel,[a] Amokrane Samira,[a] Marta Otero[b] and Moonis Ali Khan*[c]

Received 19th June 2024
Accepted 24th July 2024

DOI: 10.1039/d4ra04483e

rsc.li/rsc-advances

Besides being hazardous to humans and aquatic organisms, dyes present in water reservoirs limit sunlight's availability to aquatic plants and animals, making significant impact on their growth and development. Herein, the adsorptive removal of methylene blue (MB) dye from aqueous solution using type X (NaX) zeolite by full experimental design 2^n was studied. The physical and chemical properties of NaX zeolite were identified using various characterization techniques such as X-ray diffraction (XRD), scanning electron microscopy with energy dispersive X-ray (SEM-EDS), Fourier transform infra-red (FT-IR), and Brunauer–Emmett–Teller (BET) surface area analyses. Results confirmed that NaX zeolite had a cubic shaped crystalline structure with 2–4 μm size and high (375 $m^2\ g^{-1}$) specific surface area, having 90% optimal adsorption efficiency. Langmuir and Elovich isotherm models were best fitted to adsorption experimental data and a pseudo-second-order kinetic model describes well the adsorption kinetic data. Akaike information criteria (AIC) was used to assess the best fitted models on the experimental data. A thermodynamic study reveals that the MB adsorption onto NaX was exothermic, spontaneous, and feasible.

1. Introduction

Different industrial establishments generate specific types of waste. These wastes, when discharged into watercourses, have damaging repercussions on humans and environmental health.[1,2] One example of such discharges manifests in the form of toxic dyes that contaminate aquatic environments.[3] Water, being the fundamental element of life, constitutes an invaluable resource. However, in recent decades, demographic growth and industrial development have had a detrimental environmental impact,[4] particularly through a massive discharge of dyes into water bodies.[5] Among these dyes, methylene blue (MB), classified as carcinogenic and hazardous to humans, is of concern because of its uncontrolled discharge from many industries.[6]

Researchers have used various treatment technologies, such as ion-exchange,[7] chemical precipitation,[8] membrane processes,[9] filtration,[10] photocatalysis,[11] solvent extraction,[12] and adsorption[5] to remove pollutants from water.[13,14] Among them, adsorption stands out for its simplicity, affordability, ease of handling, and recyclability.[15] Therefore, several authors in their current research have focused on developing methods to protect aquatic environments using adsorbents with a high adsorption capacity.[15–19] Among adsorbents, synthetic and natural zeolites, due to their ability to adsorb drugs, pesticides, pharmaceuticals, metal ions, and dyes have been widely explored.[20–22] Andrunik *et al.*[20] tested the potential of fly ash-based zeolites and zeolite-carbon composites to remove pesticides from water. Amokrane *et al.*[21] revealed that zeolites X and Y have better nitrogen adsorption capacity, unlike zeolite A. Senila *et al.*[22] reviewed and summarized previous research into the modification of zeolites to improve their adsorption capacity, showing that natural zeolites can reduce costs and pollution compared with synthetic adsorbents. Synthetic zeolites are produced from mixtures of silicon and aluminum in basic or acidic media at temperatures ranging from 100 to 200 °C and under autogenous reactions.[23] They have undeniable advantages,[24] including reasonable processing costs, great versatility, and unique properties, such as their specific surface area and porosity, which give them an excellent capacity for adsorbing different types of pollutants.[25,26] Zouaoui *et al.*[25] showed that high-pressure CO_2 adsorption on NaX, LiX, KX, ZnX and MgX zeolites varies as a function of exchange ions and temperatures. They found that the Na^+ exchange with Li^+ improves adsorption capacity by increasing pore volume and specific surface area, while exchange with Zn^{2+}, Mg^{2+} and K^+ decreases these parameters.

[a]*Laboratory of Materials Technology, University of Science and Technology Houari Boumediene, B. P. 32, El-Alia, Bab-Ezzouar, Algiers, Algeria*

[b]*Departmento de Química y Física Aplicadas, Universidad de León, Campus de Vegazana s/n, 24071 León, Spain*

[c]*Chemistry Department, College of Science, King Saud University, Riyadh 11451, Saudi Arabia. E-mail: mokhan@ksu.edu.sa*

† Electronic supplementary information (ESI) available. See DOI: https://doi.org/10.1039/d4ra04483e

Zeolites are known to have the following composition: $[M]_{x/z}^{n+}[(SiO_2)_x(AlO_2^-)_y]mH_2O$ (M: compensating ions, n: valency, x and y: molar fractions and m: number of water molecules).[27] They have a cubic framework supported by silica and alumina tetrahedral units resulting in a net negative charge that is compensated by alkali ions. This three-dimensional network consisting a channel/void system which offers large possibilities for dyes and heavy metal ions to diffuse and exchange onto zeolite surfaces.[23] Among zeolites, NaX is known by a super cage (13 Å) and external pores (8 Å), which are capable to contain and adsorb many organic or inorganic elements.[28] Lin *et al.*[29] synthesized a first aluminosilicate zeolite (ZEO-1) with multidimensional pores (up to 10 × 10 Å) and an interconnected supercages. Furthermore, Li *et al.*[30] studied ZEO-3 and found that it exhibited exceptional performance in the reduction and recovery of volatile organic compounds, outperforming that of other zeolites and MOFs. Gao *et al.*[31] reported that aluminosilicate zeolites with extra-large pores, could process bulky molecules and a new silicate chain expansion strategy, creates three-dimensional zeolites and efficient catalysts for alkene oxidation.

Although, previous studies have examined the effectiveness of zeolites in the adsorption of various pollutants, including heavy metals and dyes,[19,32] very few have looked at the use of NaX zeolite for MB adsorption.[33,34] Moreover, to the best of authors' knowledge, the optimization of the experimental conditions for MB adsorption onto NaX zeolite by an experimental design has never been reported. In this context, the current work demonstrated the ability of NaX zeolite synthesized by a hydrothermal process to remove the basic dye MB from an aqueous solution. The zeolite sample was subjected to various characterizations including X-ray diffraction (XRD), scanning electron microscopy (SEM), energy dispersive spectroscopy (EDS), Fourier transform infrared spectroscopy (FTIR) and Brunauer–Emmett–Teller (BET) surface area analyses. In addition, the MB adsorption onto the zeolite was described through isotherm, kinetic, and thermodynamic parameters. To reduce the number of trials and associated costs, parametric optimization using a full factorial design 2^4 was performed. This rigorous and efficient methodological approach enabled us to determine the optimum conditions for MB adsorption onto NaX zeolite, highlighting the importance of full factorial designs for such a purpose.

2. Experimental

2.1. Chemical and reagents

All the chemicals used during the study were analytical reagent (AR) grade or as reported. Methylene blue (MB) was procured from Sigma-Aldrich, Hydrochloric acid (HCl, 37%) and sodium hydroxide (NaOH, >99%) were purchased form Fluka. Silica (100% purity) was purchased from Prolabo. Aluminum isopropoxide (98% purity) was procured from Merck. To prepare solutions and to wash glassware, deionized (DI) water was used.

2.2. Synthesis procedure of NaX zeolite

The NaX zeolite with molar composition $4.8Na_2O$, $1Al_2O_3$, $3.8SiO_2$, $224H_2O$ was synthesized using a previously reported protocol.[35] Briefly, a solution of sodium hydroxide (2.1 g) in DI water (21.6 g) was added to fumed silica (4.18 g), and the mixture was mechanically stirred for 2 h. Thereafter, aluminum isopropoxide (2.2 g) was gradually added under continuous stirring for 2 h, and the obtained gel was kept for incubation over 24 h to promote crystallization and complete the reaction for zeolite formation. The hydrothermal reaction was carried out in Teflon-lined stainless-steel autoclave at 100 °C for 24 h. The powder product was recovered by filtration, washed with DI water and overnight dried at 100 °C. Finally, the sample was calcined by heating at 300 °C in an air atmosphere for 6 h to get the NaX zeolite.

2.3. MB adsorption procedure

Batch adsorption experiments were conducted in 500 mL Erlenmeyer flasks by stirring 200 mL of MB solution with varied initial concentration (from 5 to 120 mg L^{-1}) together with NaX zeolite (0.04 to 0.7 g). The pH was monitored using a Hanna pH meter and adjusted using HCl and NaOH solutions. Aliquots (1 mL) were collected at regular time intervals and the solid/solution phases were separated through centrifugation. The absorbance of the supernatant solution was measured at λ_{max} (665 nm) by UV-visible spectrophotometer (Optizen 2120 UV).

The MB uptake percentage (%), adsorbed mass at the equilibrium (q_e) and adsorbed mass any time t (q_t) on NaX zeolite were respectively evaluated as:

$$\text{Adsorption uptake } (\%) = \frac{(C_0 - C_e)}{C_0} \times 100 \quad (1)$$

$$q_e = \frac{(C_0 - C_e)}{m} \times v \quad (2)$$

$$q_t = \frac{(C_0 - C_t)}{m} \times v \quad (3)$$

where C_0, C_e, and C_t are the initial, equilibrium and at any time t concentrations of MB, respectively, m (g) is the adsorbent mass and v (L) is the volume of the solution.

2.4. Characterization of NaX zeolite

The XRD (Philips PW 1710 diffractometer) analysis was carried out to identify the NaX zeolite structure. The surface morphology and elemental content of synthesized NaX zeolite was analysed by SEM coupled with EDX (XL-20 equipment) analysis. The chemical functionalities present on NaX zeolite surface were studied through FTIR (Nicolet iS10 spectrometer) analysis, and the specific surface area and pore volume of NaX zeolite were calculated through BET analysis of N_2 adsorption–desorption results (Micromeritics ASAP 2010).

2.5. Optimization of adsorption experiments

A full two-level factorial design with 4 factors and therefore involving 16 experiments was employed to optimize the experimental conditions for MB adsorption onto NaX zeolite. The considered experimental factors were pH, solid/liquid ratio (S/L), initial concentration and temperature, while the MB

adsorption percentage was the response variable. A mathematical model that accurately describes the experimental process and optimizes the operating parameters was developed using the method of least squares to fit the data.[36] An analysis of variance (ANOVA) was also performed to determine the significance of the factors and their interactions. The experimental conditions are listed in Table S1.† An empirical regression equation with four parameters and their interactions as shown in the eqn (4) was derived.

$$\text{Adsorption uptake (\%)} = b_0 + b_1x_1 + b_2x_2 + b_3x_3 + b_4x_4 + b_{12}x_1x_2 + b_{13}x_1x_3 + b_{14}x_1x_4 + b_{23}x_2x_3 + b_{24}x_2x_4 + b_{34}x_3x_4 + b_{123}x_1x_2x_3 + b_{124}x_1x_2x_4 + b_{134}x_1x_3x_4 + b_{234}x_2x_3x_4 + b_{1234}x_1x_2x_3x_4 \quad (4)$$

where b_0, b_1, b_2, b_3 and b_4 are the linear coefficients; b_{12}, b_{13}, b_{14}, b_{23}, b_{24}, b_{24} and b_{34} are the second-order interaction terms; b_{123}, b_{124}, b_{134} and b_{234} are the third-order interaction terms and b_{1234} is the fourth-order interaction term. x_1, x_2, x_3 and x_4 are the dimensionless coded factors, as displayed in Table S1† (pH, initial MB concentration, S/L and temperature, respectively).[37] The levels −1 and 1 represent the low and high levels, respectively, for each factor.

3. Results and discussion

3.1. Characterization of NaX zeolite

The XRD patterns of the here synthesized NaX zeolite is illustrated in Fig. 1a. The patterns correspond to the faujasite NaX structure, with a strong peak in the 2θ ranges of 5–30°, indicating successful synthesis of the microporous NaX zeolite structure. The main phase observed was consistent with previous literature[35] and all planes were compared with those in crystallographic databases[28,38] and identified as NaX structure. As shown in Fig. 1a, all the peaks were Miller-indexed (*hkl*), showing the important (111) plane with high intensity and belonging to the structure of NaX zeolite.

Morphologically, NaX zeolite have cubic shaped crystals with an average dimension of about 2–4 μm, illustrated in Fig. 1b. The elemental composition of NaX zeolite showed that the main atoms Si and Al, together with the compensating Na, constitute the framework structure (Table S2†). The mass ratio of Si/Al was found to 1.198%, which corresponds to the synthesized NaX zeolite and was near to reported range (1.1–1.5).[39] These results were in agreement with previous reports on NaX zeolites synthesized by other authors.[35,40]

FTIR spectrum of NaX zeolite highlights all absorption bands of different bonds attributed to its framework structure (Fig. 1c) in the frequency range from 4000 to 500 cm^{-1}. Two important zones were defined in this spectrum, which revealed the functionalized groups (3880–3500 cm^{-1}) and topological structure (1200–500 cm^{-1}) as reported in the literature.[27,41] The bands of the first zone of frequencies between 3880 and 3750 cm^{-1} were attributed to silanol (Si–OH) groups and to probable impurities. The bands at 3650 and 3500 cm^{-1} were assigned to the high and low frequencies of hydroxyl groups (O–H), respectively.[41] The high frequency (HF) bands were found in

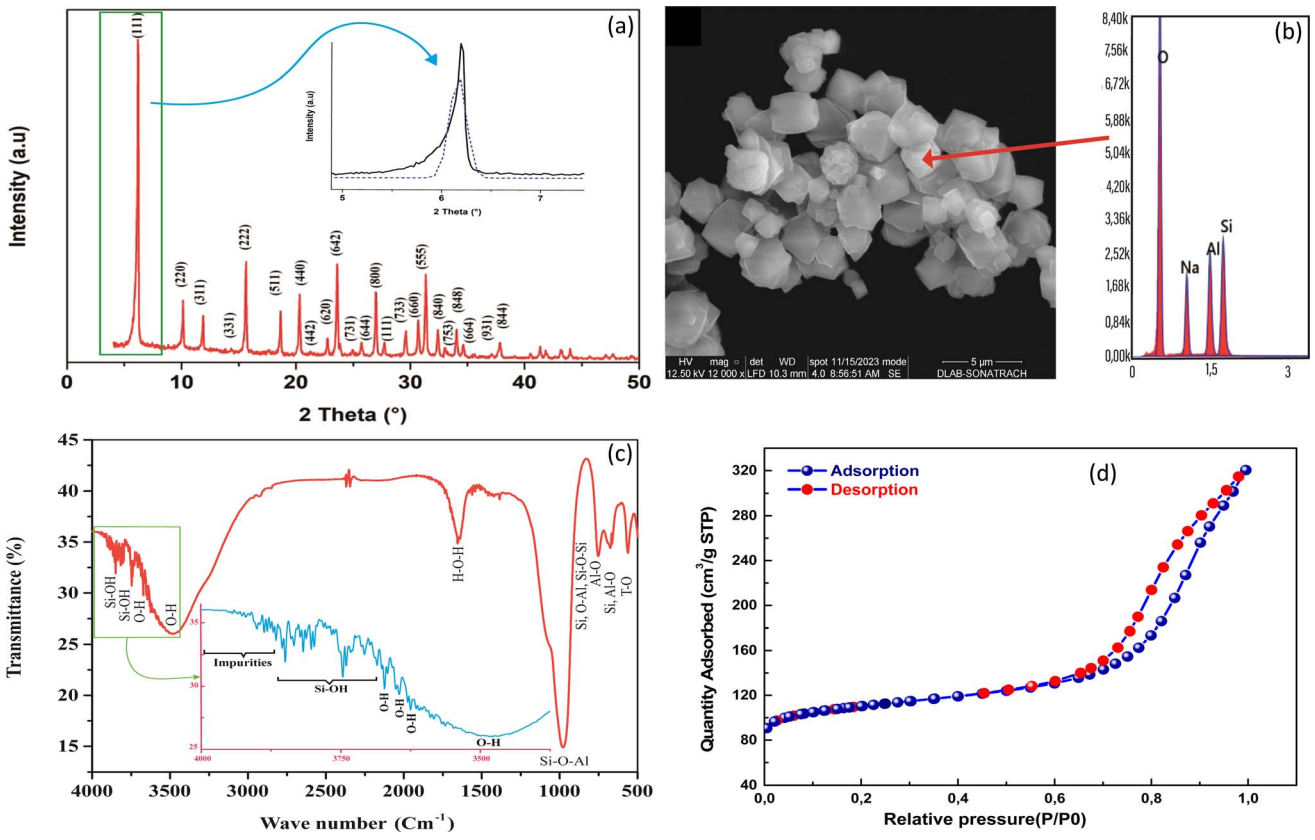

Fig. 1 XRD pattern (a), SEM micrograph and EDX spectrum (b), FTIR spectrum (c) and N_2 adsorption/desorption isotherms of NaX zeolite.

the super cages of NaX zeolite (13 Å), in accordance to previous works of Breck[27] and Nibou *et al.*[41] that reported the localization of these HF bands and consequently facilitate the adsorption of MB molecules. In the second zone, the band at 989 cm^{-1} was due to the asymmetric elongation of Si–O–Al bond; the band at 755 cm^{-1} was associated with the symmetrical vibrations of Si–O–Al and Si–O–Si bonds; that at 679 cm^{-1} was assigned to the symmetrical vibration of Al–O bond; the absorption band at 565 cm^{-1} was characteristic to the double rings (DR) of NaX zeolite; and that at 510 cm^{-1} was assigned to the vibration deformation of the T–O (T; Si or Al) bond. Another absorption band was also observed at 1633 cm^{-1}, corresponding to the vibration of the H–O–H bond of water molecules.

The specific surface area (SSA) and micropore volume of the synthesized NaX zeolite were determined by BET surface area analysis through N_2 adsorption/desorption (Fig. 1d). The results revealed a high SSA of 375 $m^2\ g^{-1}$ with respective microporous and external surfaces of about 255.3 and 119.7 $m^2\ g^{-1}$. The obtained micropore volume of synthesized NaX was 0.120 $cm^3\ g^{-1}$. The N_2 adsorption/desorption curves (Fig. 1d) showed the presence of hysteresis,[27] indicating a mesoporous volume of 0.20 $cm^3\ g^{-1}$. The N_2 maximum quantity adsorbed onto NaX using BET method was 0.320 $cm^3\ g^{-1}$ (at $P/P_0 = 0.99$). These results indicate that the textural properties of the synthesized NaX zeolite are favorable for the uptake of MB, with a large number of sites available for its adsorption.

3.2. Adsorption performance of NaX zeolite

3.2.1. Effect of contact time and MB initial concentration. Results on the uptake (%) of MB along time at the different initial concentration considered (from 5 to 120 mg L^{-1}) are depicted in Fig. 2a. At the lower MB initial concentration range (5–20 mg L^{-1}), more than 80% MB was adsorbed within 25 min. Meanwhile, at relatively high MB initial concentrations (50–120 mg L^{-1}) less than 50% MB was adsorbed within 25 min. In all cases, adsorption was faster at the initial stage, which was more evident for experiments carried out at lower MB initial concentration due to the availability of a large number of active binding sites. However, at relatively high initial MB concentration, due to the quick saturation of adsorption sites on NaX zeolite surface, the uptake was slow. Overall, the equilibration time for the studied concentration range was 60 min, illustrated in Fig. 2a.

On the other hand, as it may be seen in Fig. 2a, the MB uptake percentage mostly decreased with the increase of the initial MB concentration from 5 to 120 mg L^{-1}. Exceptionally, at the lowest concentrations (5–10 mg L^{-1}), an increase of MB uptake percentage was observed with increasing initial concentration. This could be explained by the limited availability of MB molecules at very low initial concentrations, which may have limited their interaction with NaX sites. However, at concentrations higher than 20 mg L^{-1}, a decrease in MB uptake with increasing initial concentration was observed in all cases.

Similar results on MB adsorption onto different adsorbents were observed by other authors. For example, Kuang *et al.*[42] studied the adsorption of MB onto surfactant modified activated carbon and noticed that the uptake percentage decreased from 96.6 to 58.7% with an increase in the initial dye concentration from 10 to 50 mg L^{-1}, while the adsorption capacity of the dye increased under the same conditions. Yagub *et al.*[43]

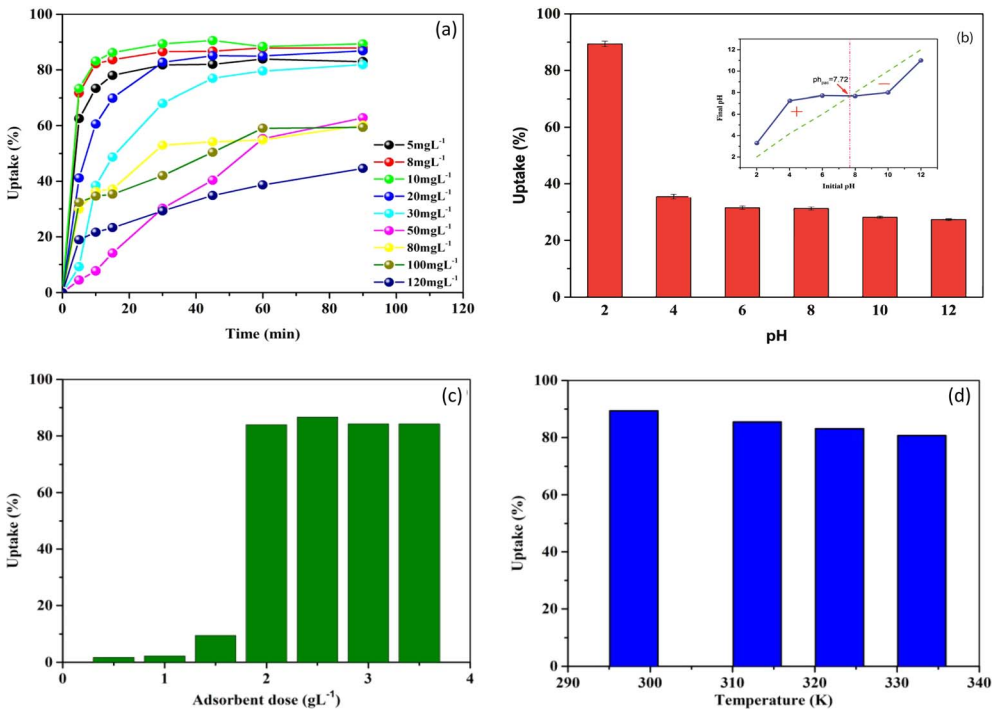

Fig. 2 Effect of contact time at varied initial concentrations (a), pH (b), solid/liquid ratio (c), and temperature (d) on MB adsorption onto NaX zeolite.

studied the adsorption of MB onto pine leaves with an equilibrium time of 240 min and found that, when the MB concentration was increased from 10 to 90 mg L^{-1}, the dye removal percentage decreased from 96.5 to 40.9%.

3.2.2. Effect of initial pH. The pH of the dye solution is a crucial factor that affects the adsorption capacity.[44] It can change: (1) the surface charge of the adsorbent, (2) the degree of ionization of the adsorbate molecule, and (3) the extent of dissociation of the functional groups on the active sites of the adsorbent.[45,46] During current study, the pH was varied from 2 to 12, while concentration, S/L, and temperature were kept constant at 10 mg L^{-1}, 2.5, and 298 K, respectively. The obtained results, which are displayed in Fig. 2b, showed a high uptake percentage (90%) at pH 2. Then, at pH 4, an uptake ~35% was determined, observing a slightly decreasing trend with increasing pH until reaching ~27% at pH 12. These results were in line with published results on the MB adsorption onto different zeolites[47] and confirmed the significance of pH on the adsorption of organic and inorganic pollutants on zeolitic materials.[48]

The point of zero charge (pH_{pzc}) corresponds to a neutral surface charge. Below the pH_{pzc}, the surface becomes positively charged, attracting anions and repelling cations.[5,40] During the current study, it was difficult to provide a definitive explication for the effect of pH on MB adsorption based solely on the pH values considered in relation to this pH_{pzc}, which was determined to be 7.72 (Fig. 2b, inset). The increase in adsorption under acidic conditions may be due to the preference of dye cations for active sites and/or increased accessibility to interlayer regions of protonated ($MB\ H^{2+}$) and monomeric species resulting from the removal of certain oxides from the NaX zeolite surface.

The MB adsorption capacity was highest at pH 2, where the surface charge of the particles was positively charged. This suggests that a negatively charged surface appears after the removal of certain species as $[Al(OH)_4]^-$ and $Al(OH)_3$ from NaX zeolite, leading to efficient adsorption of protonated and monomeric MB species. In contrast, to the decreasing tendency of oxide removal with increasing pH, alkali cations and other exchangeable metals on the surface and in the interlayer region of NaX zeolite undergo hydration creating a hydrophilic environment.[49,50] This can also lead to a decrease in MB adsorption provided that the surface charge of the zeolite tends towards zero.

3.2.3. Effect of solid/liquid ratio. The effect of S/L on the adsorption of MB onto NaX zeolite was examined. The experimental conditions were pH 2, initial MB concentration of 10 mg L^{-1}, and 298 K, which were kept constant while the S/L varied from 0.5 to 3.5. The obtained results are presented in Fig. 2c, which shows very low adsorption uptake percentages (below 8%) for ratios 0.5, 1, and 1.5. This is due to the limited number of active sites available on NaX zeolite at very low S/L. In contrast, higher and quite similar yields around 90% were observed for ratios of 2, 2.5, 3 and 4. These results are explained by the fact that, as the S/L increases, the amount of zeolite increases, resulting in an increase in the active surface area of NaX for adsorption.[51,52] Since the MB concentration was maintained constant, for ratios equal or larger than 2, the adsorption uptake percentage was stabilized due to the saturation attributed to the occupation of the active sites and equilibration with the liquid phase. These results were in line to those observed by Wahyuni *et al.*,[19] that reported the impact of the S/L for MB removal from water using recoverable natural zeolite/Fe_3O_4 adsorbent, showing a yield up to 25 mg/100 mL, but beyond this quantity, no significant increase was observed due to the saturation of the solution that limits interaction with the adsorbent surface.

3.2.4. Effect of temperature. The adsorption of MB onto NaX zeolite was carried out at varied temperatures (298, 313, 323, and 333 K), while the parameters such as pH, initial concentration, and S/L were kept constant at their optimal values (Fig. 2d). The results revealed that the uptake percentage decreases from 89 to 80% as the temperature increases from 298 to 333 K. This suggests that the optimal temperature for these experiments was 298 K and the process was exothermic. According to these results, it may be inferred that uptake of MB from water by NaX zeolite occurs by physical adsorption.

3.3. Adsorption modeling

3.3.1. Adsorption isotherm modelling. Langmuir,[53] Freundlich,[54] Temkin,[55] and Elovich[56] isotherm models, presented in Table S3,† were applied to MB adsorption data on NaX zeolite. Fig. S1† displayed experimental results together with non-linear fittings to the referred adsorption isotherm models. The selection of best fitted isotherm was carried out by considering error functions (Table S4†) such as R^2, Adj. R^2, RSS, MSE, χ^2, RMSE, as well as AIC and AICc, so to select the model offering minimum deviations between the experimental and fitted results. Table 1 presents fitted parameters for each of the considered isotherms and the corresponding error functions.

As in may be seen in Table 1, the error functions, indicate that the Elovich isotherm model provided the best fittings to MB adsorption equilibrium data on NaX zeolite, followed by Temkin, Freundlich, and Langmuir isotherm models. A comparison between the error functions obtained by the linear and non-linear regression methods revealed a difference in errors for the non-linear method, apart from the Temkin isotherm model, where the error functions remain unchanged. This observation could be explained by a marked similarity between the linear and non-linear formulations of this model.

From Table 1, Langmuir and Elovich isotherm models appear the best suited to represent the experimental data with relatively high R^2, Adj.R^2 values and the lowest errors. Previous studies[23,57] have pointed out that the application of linear regression often leads to values of q_e that diverge considerably from the experimentally determined values. Comparing the experimental and predicted isotherms of MB adsorption on the two models it was clear that Langmuir was the best fitted model. The values of q_{mL} were 24.39 and 23.10 mg g^{-1} for linear and non-linear isotherm models, respectively. These values were considerably near to the experimentally determined value (21.61 mg g^{-1}). However, the values of q_{mE} for linear and non-linear isotherm models were 9.10 and 5.45 mg g^{-1}, respectively. There values were lower compared to Langmuir model. In

Table 1 Linear and non-linear isotherm models parameters and error functions for MB adsorption onto NaX zeolite

Parameters	Langmuir	Freundlich	Temkin	Elovich
Linear isotherm models				
	q_{mL}: 24.39 mg g^{-1} K_L: 0.12 L mg^{-1}	K_F: 3.01 mg g^{-1} n: 1.97	B: 571.16 J mol^{-1} K_T: 1.82 L mg^{-1}	q_{mE}: 9.10 mg g^{-1} K_E: 0.43 L mg^{-1}
Error functions				
R^2	0.9949	0.9602	0.9870	0.9416
Adj.R^2	0.9881	0.9109	0.9706	0.8704
SSE	0.0897	0.5504	12.7122	56.0079
χ^2	0.0149	0.0786	1.8160	8.00113
MSE	0.0149	0.0786	1.8160	8.00113
RMSE	0.1223	0.2804	1.3476	2.8286
AIC	−37.4795	−21.1498	7.1080	20.4544
AICc	−35.4795	−19.1498	9.1081	22.4544
Non-linear isotherm models				
Parameters	q_m: 23.10 mg g^{-1} K_L: 0.12 L mg^{-1}	K_F: 3.89 mg g^{-1} n: 2.38	B: 571.19 J mol^{-1} K_T: 1.83 L mg^{-1}	q_{mE}: 5.45 mg g^{-1} K_E: 0.75 L mg^{-1}
Error functions				
R^2	0.9581	0.9716	0.9742	0.9776
Adj.R^2	0.9521	0.9676	0.9705	0.9745
SSE	20.6660	13.9783	12.7122	11.0190
χ^2	2.95233	1.9969	1.8160	1.5741
MSE	2.9523	1.9969	1.8160	1.5741
RMSE	1.7182	1.4131	1.3476	1.2546
AIC	11.4815	7.9625	7.1080	5.8215
AICc	13.4815	9.9625	9.1080	7.8215

addition, the lower values of (AIC) (−37.4795) and $(AIC)_c$ (−35.4795) (Table 1) affirmed the selection of the Langmuir isotherm model as the best fitted model. A non-dimensional (R_L) known by Langmuir separation factor (R_L) was calculated to approve the MB adsorption process onto NaX. The results in Table S5† revealed that the values of R_L were <1, indicating that the adsorption process was effectively favorable.

3.4. Adsorption kinetic modelling

Pseudo-first-order (PFO) and pseudo-second-order (PSO) kinetic models[57,58] for MB adsorption onto NaX zeolite were carried out by varying the initial MB concentrations from 5 to 120 mg L^{-1} and the temperature from 298 to 333 K. Fig. S2† presents the linearized experimental kinetic results for the adsorption of MB onto NaX zeolite. Tables 2 and 3 display the fitted parameters and the corresponding error functions, AIC, and AICc criteria. The best-fit kinetic model was selected based on higher R^2, lower AIC and AICc criteria values and the error functions that produced minimum error distribution between the experimental and predicted values. The slopes and intercepts of plots of the linear representations (Fig. S2†) were obtained to determine the rate constants and equilibrium adsorption amount q_e of kinetic models.

Tables 2 and 3 showed that PSO model had higher R^2 values than PFO model. Additionally, the error function, AIC, and AICc criteria of the PSO model had lower values than those of the PFO model for the entire range of experimental data. Based on these results, the PSO model was the most suitable among the considered models to describe MB adsorption data onto NaX zeolite. This was further confirmed by nearer $q_{e,exp}$ and $q_{e,cal.}$ values, suggesting that the rate-limiting step could correspond to a chemisorption process.

To verify the nature of adsorption process, activation energy (E_a) was determined by using the Arrhenius' equation by a plot between ln k_2 and $1/T$ (figure not given).[58]

$$k_2 = A_0 \exp\left(-\frac{E_a}{RT}\right) \quad (5)$$

The determined E_a magnitude for MB adsorption on NaX zeolite was 0.0084 kJ mol^{-1}, suggesting physical nature of adsorption process.

3.5. Adsorption thermodynamic modelling

The thermodynamic modelling parameters such as standard free energy change (ΔG°), standard enthalpy change (ΔH°), and standard entropy change (ΔS°)[59] were obtained from the following equations:

$$\ln K_C = \left(\frac{\Delta S^\circ}{R}\right) - \left(\frac{\Delta H^\circ}{RT}\right) \quad (6)$$

$$\Delta G^\circ = \Delta H^\circ - T\Delta S^\circ \quad (7)$$

Eqn (6)[60] relates the equilibrium constant K_c to the values of ΔS° and ΔH° and the universal gas constant (R), while eqn (7) expressed the relation between ΔG°, ΔH°, and ΔS° in terms of temperature (K).

Analyzing the ln K_c plot using eqn (6) as a function of ($1/T$) (Fig. S3†) allowed the determination of ΔH° and ΔS° by using

Table 2 PFO kinetic parameters and error functions for MB adsorption onto NaX zeolite

Initial concentration (C_0, mg L^{-1})	$q_{e,exp.}$ (mg g^{-1})	$q_{e,\ cal.}$ (mg g^{-1})	$K_1 \times 10^2$ (1/min)	R^2	Adj.R^2	SSE	χ^2	MSE	RMSE	AIC	AICc
5	1.658	0.703	9.5	0.937	0.848	1.831	0.458	0.458	0.677	−10.332	−8.332
8	2.812	1.191	11.1	0.940	0.86	4.918	0.984	0.984	0.992	−1.439	0.561
10	3.574	2.922	9.44	0.825	0.575	3.741	1.247	1.247	1.117	−3.901	−1.901
20	6.949	5.038	8.3	0.951	0.885	1.341	0.268	0.268	0.518	−13.138	−11.138
30	9.829	10.740	6.1	0.997	0.993	0.067	0.013	0.013	0.116	−40.080	−38.080
50	12.56	15.768	3.4	0.966	0.920	0.249	0.050	0.050	0.223	−28.283	−26.283
80	17.559	25.053	1.2	0.854	0.675	0.186	0.037	0.037	0.193	−30.916	−28.916
100	21.618	32.298	1.1	0.858	0.684	0.021	0.004	0.004	0.065	−50.459	−48.459
120	21.412	16.710	2.9	0.979	0.951	0.109	0.022	0.022	0.148	−35.700	−33.705
***T* (K)**											
298	3.574	2.54	6.2	0.825	0.575	3.74	1.247	1.247	1.117	−3.901	−1.901
313	3.420	0.42	5.4	0.912	0.798	3.029	0.606	0.606	0.778	−5.800	−3.800
323	3.323	2.02	7.6	0.926	0.829	2.677	0.535	0.535	0.732	−6.913	−4.913
333	3.227	0.12	5.4	0.824	0.614	6.371	1.274	1.274	1.129	0.890	2.890

Table 3 PSO kinetic parameters and error functions for MB adsorption onto NaX zeolite

Initial concentration (C_0, mg L^{-1})	$q_{e,exp.}$ (mg g^{-1})	$q_{e,\ cal.}$ (mg g^{-1})	$K_2 \times 10^2$ (g mg min^{-1})	R^2	Adj.R^2	SSE	χ^2	MSE	RMSE	AIC	AICc
5	1.658	1.678	663.955	0.999	0.999	1.021	0.170	0.170	0.412	−15.589	−13.589
8	2.812	2.833	525.776	0.999	0.999	0.109	0.018	0.018	0.135	−35.694	−33.694
10	3.574	3.597	585.485	0.999	0.999	0.146	0.024	0.024	0.156	−33.069	−31.069
20	6.949	7.143	47.689	0.999	0.997	0.383	0.064	0.064	0.253	−24.402	−22.402
30	9.829	11.765	4.643	0.944	0.874	9.826	1.638	1.638	1.280	4.790	6.790
50	12.559	14.493	2.542	0.717	0.432	50.24	8.374	8.374	2.894	19.477	21.477
80	17.559	20	9.579	0.977	0.947	0.343	0.069	0.069	0.262	−25.400	−23.400
100	21.618	23.810	6.945	0.978	0.947	0.241	0.048	0.048	0.219	−28.591	−26.591
120	21.412	22.728	4.059	0.989	0.947	0.492	0.082	0.082	0.286	−22.159	−20.159
***T* (K)**											
298	3.574	3.597	3.597	0.999	0.999	0.146	0.024	0.024	0.156	−33.069	−31.069
313	3.420	3.436	3.436	0.999	0.999	0.064	0.011	0.011	0.103	−40.537	−38.537
323	3.324	3.344	3.344	0.999	0.999	0.143	0.024	0.024	0.154	−33.294	−31.294
333	3.228	3.236	3.237	0.999	0.999	0.013	0.002	0.002	0.047	−54.867	−52.867

the slope and intercept of the curve; the results are summarized in Table 4. Thermodynamic parameters analysis revealed that the MB dye adsorption onto NaX was spontaneous reaction ($\Delta G° < 0$), indicating a natural process occurrence. As temperature increases, the values of $\Delta G°$ become less negative, suggesting a decrease in the adsorption capacity, making adsorption thermodynamically favorable. The negative value of $\Delta H°$ confirms that MB adsorption onto NaX was an exothermic process. Furthermore, the negative value of $\Delta S°$ implies a reduction in disorder at the solid–liquid interface during dye adsorption, attesting to the dye's stability on the NaX surface.

4. Determination of factors and modelling

4.1. Modelling uptake based on experimental parameters

Table 5 summarizes the experimental matrix containing the experimental conditions for each trial and the corresponding experimental results of MB adsorption uptake ($uptake_{exp.}$ (%)). These results were obtained by various combinations of the factors: pH, S/L, initial concentration, and temperature. Analysis of the results revealed that the minimum adsorption uptake was found under the conditions of trial no. 14, *i.e.*, for the following conditions: pH = 12, S/L ratio = 0.5, initial concentration = 120 and temperature = 60 °C. Meanwhile, the maximum uptake was observed in trial no. 3 with pH = 2, S/L ratio = 3.5, initial concentration = 5 and temperature = 25 °C.

4.2. Calculation of effects

To calculate the main effects and interactions among the factors x_1, x_2, x_3, and x_4, an effects matrix has been included. This matrix, along with the coefficient values of the regression equation for the calculation of the modelled uptake ($uptake_{mod.}$ (%)) is given as:

$$\text{Uptake (\%)} = 23.896 - 14.233\text{pH} + 15.904r\ \text{(s/l)} - 3.955C_0 - 1.873T - 12.814\text{pH} \times r\ \text{(s/l)} - 4.370\text{pH} \times C_0 + 0.844\text{pH} \times T - 5.086r\ \text{(s/l)} \times C_0 - 1.187r\text{(s/l)} \times T + 0.674C_0 \times T + 3.278\text{pH} \times r\ \text{(s/l)} \times C_0 + 0.664\text{pH} \times r\ \text{(s/l)} \times T + 0.078\text{pH} \times C_0 \times T + 0.600r\ \text{(s/l)} \times C_0 \times T - 0.3005\text{pH} \times r\ \text{(s/l)} \times C_0 \times T \quad (8)$$

Table 4 Thermodynamic parameters for MB adsorption onto NaX zeolite

		$\Delta G°$ (kJ mol^{-1})			
$\Delta H°$ (kJ mol^{-1})	$\Delta S°$ (kJ mol^{-1} K^{-1})	298 K	313 K	323 K	333 K
−16.478	−0.0453	−2.964	−2.737	−2.284	−1.831

Table 5 Factorial design matrix for MB adsorption on NaX

No.	Configuration	x_1(pH)	x_2(S/L ratio)	$x_3(C_0)$	$x_4(T)$	Uptake$_{exp.}$ (%)
1	− − − −	−1	−1	−1	−1	1.19
2	+ − − −	1	−1	−1	−1	14.05
3	− + − −	−1	1	−1	−1	80.86
4	+ + − −	1	1	−1	−1	25.49
5	− − + −	−1	−1	1	−1	19.36
6	+ − + −	1	−1	1	−1	0.11
7	− + + −	−1	1	1	−1	61.97
8	+ + + −	1	1	1	−1	3.1210
9	− − − +	−1	−1	−1	1	0.07
10	+ − − +	1	−1	−1	1	12.13
11	− + − +	−1	1	−1	1	68.73
12	+ + − +	1	1	−1	1	20.28
13	− − + +	−1	−1	1	1	17.02
14	+ − + +	1	−1	1	1	0.001
15	− + + +	−1	1	1	1	55.83
16	+ + + +	1	1	1	1	2.12

To compare the measured responses (uptake$_{exp.}$ (%)) with the estimated responses (uptake$_{mod.}$ (%)), the adequacy graph has been plotted. Fig. 3 showed that the estimated responses were placed on the *x*-axis, and the measured responses were on the *y*-axis. The coefficient of determination (R^2) equals 99.99%, indicating that the chosen models were appropriate.

4.3. The influence of individual factors and their combinations on yield

Fig. 4 showed how each independent variable (x_1, x_2, x_3, and x_4) affects the dependent response using the experiment matrix and the regression equation. A positive impact on uptake (%) was manifested for S/L. This observation suggests that the efficiency of the adsorption process was intensified by increasing this ratio.

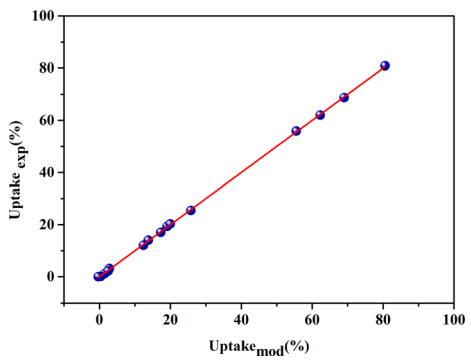

Fig. 3 Plot of experimental *versus* predicted data of MB adsorption.

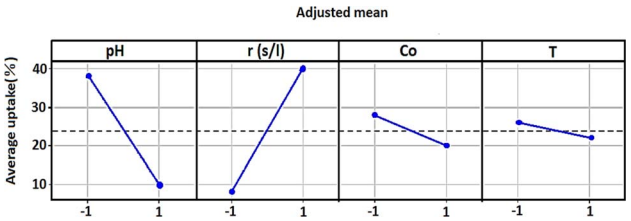

Fig. 4 Plots of four independent variables for MB adsorption onto NaX zeolite.

Conversely, negative effects on uptake (%) were exhibited by factors such as pH, concentration, and temperature, implying that high levels of these parameters were associated with a decrease in performance. In order to analyse if there is interaction between the considered experimental variables, the responses generated at the two levels (low and high) of each factor were measured. If the responses of two factors show an inverse variation, this indicates an interaction between them. More precisely, this interaction was observed when the two lines representing the respective variations in responses were not parallel. Fig. 5 graphically illustrates the obtained plots for each factor on the adsorption uptake. The interactions examined relate to the combination of the four variables and their influence on the response. Some of these interactions produced positive effects, while others had a negative impact on the course of the adsorption process.

As it may be seen in Fig. 5, there are marked interaction effects between pH and S/L, as well as between the initial dye concentration and the pH and S/L. However, the interaction between temperature and the other three variables was not significant.

4.4. Analysis of variance (ANOVA)

Significance verification is crucial to assessing the relevance of variables effects and of their interactions. Obtaining an adequate number of degrees of freedom for residues is essential as this allows precise estimation of residual variance (Table 6) and enhancing the reliability of hypothesis tests.

In the case where the degrees of freedom for residues are zero (in cases where $n = p$, *i.e.*, the number of parameters is equal to the number of observations), it becomes impossible to conduct hypothesis tests on residual effects as there is no freedom available to estimate residual variance. To solve this problem, an interaction was eliminated, leading to a simplification of the model equation as follows:

$$\text{Uptake (\%)} = 23.896 - 14.233\text{pH} + 15.904r\ (\text{s/l}) - 3.955C_0 - 1.873T - 12.814\text{pH} \times r\ (\text{s/l}) - 4.370\text{pH} \times C_0 + 0.844\text{pH} \times T - 5.086r\ (\text{s/l}) \times C_0 - 1.187r\ (\text{s/l}) \times T + 0.674C_0 \times T + 3.278\ \text{pH} \times r\ (\text{s/l}) \times C_0 + 0.664\text{pH} \times r\ (\text{s/l}) \times T + 0.078\text{pH} \times C_0 \times T + 0.600r\ (\text{s/l}) \times C_0 \times T \quad (9)$$

To assess the significance of the effects, the Student's *t*-test was used with a significance threshold of 0.05. Critical test

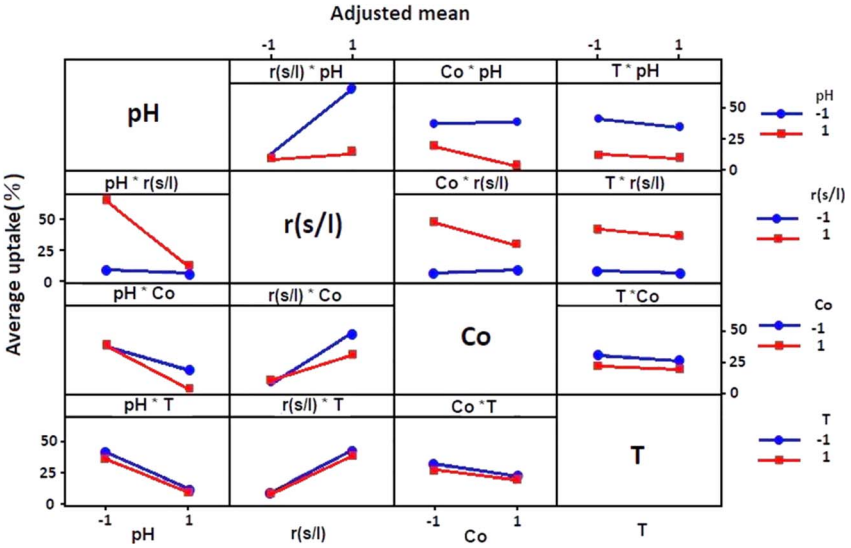

Fig. 5 Interaction plot of four independents variable of MB adsorption onto NaX zeolite.

Table 6 Values of residuals and squares of residuals for the uptake (%)

No.	$Uptake_{exp.}$ (%)	$Uptake_{mod.}$ (%)	e_i	e_i^2
1	1.19	1.49	−0.30054375	0.090326546
2	14.05	13.75	$-e_i$	e_i^2
3	80.86	80.56	$-e_i$	e_i^2
4	25.49	25.79	e_i	e_i^2
5	19.36	19.06	$-e_i$	e_i^2
6	0.11	−0.41	e_i	e_i^2
7	61.97	62.29	e_i	e_i^2
8	3.12	2.82	$-e_i$	e_i^2
9	0.07	0.23	$-e_i$	e_i^2
10	12.13	12.43	e_i	e_i^2
11	68.73	69.03	e_i	e_i^2
12	20.28	19.98	$-e_i$	e_i^2
13	17.02	17.32	e_i	e_i^2
14	0.001	−0.30	$-e_i$	e_i^2
15	55.83	55.53	$-e_i$	e_i^2
16	2.12	2.42	e_i	e_i^2

values were calculated based on the number of parameters of the model at a 95% confidence level. In this context, all Student's t values below 12.706 were considered not statistically significant. The detailed results of the tests are presented in Table 7.

Analysis of the results revealed that the coefficients associated with pH, S/L, and C_0 were statistically significant ($p < 0.05$), while T was not significant ($p > 0.05$). Terms involving the squares of pH·R/L, pH·C_0, and S/L·C_0 were also significant ($p < 0.05$), while the pH·T, S/L·T, and C_0·T interactions, as well as the values implicating the interactions of pH·S/L·C_0, pH·R/L·T, pH·C_0·T, and S/L·C_0·T were non-significant ($p > 0.05$). In summary, the effect of temperature (T) was not significant, which indicates that the interactions involving temperature were not significant either. On the other hand, the other effects and interactions were significant, confirming the rejection of the null hypothesis and the presence of significant differences between averages. Considering these findings, the simplified regression equation becomes as follows:

$$\text{Uptake (\%)} = 23.896 - 14.233\text{pH} + 15.904\text{R/L} - 3.955C_0 - 12.814\text{pH} \times \text{R/L} - 4.370\text{pH} \times C_0 - 5.086\text{R/L} \times C_0 \quad (10)$$

Validation of the linear model is of crucial importance, requiring the use of various measurements such as ANOVA, SCEL (corrected average quadratic error), SECR (residual average quadratic error), SCET (total average quadratic error), and the Fisher test. These ANOVA measurements, which allow for assessing the adjustment of the linear model and ensure the reliability of the results are summarized in Table 8. The results confirm the significance of the model, with a calculated F value ($F_{calculated}$) of 551.9165, well above the critical value of F at the 5% threshold. In addition, the correlation coefficients R^2, $R_{adj.}^2$ and R_{prevu}^2 were significantly high, at 99.99%, 99.81% and 96.69% respectively. These high values indicate the adequacy of the experimental data for the proposed model.

4.5. Pareto chart

Fig. 6 presents the Pareto chart of the analysis of variances. This chart categorizes the variables and their interactions according to their increasing influence on the MB adsorption uptake (%) onto the NaX zeolite. The effects are standardized for better comparison. The standardized values in this figure are obtained by dividing the effect of each variable by the error on the estimated value of the corresponding variable. The higher the standardized effect, the more considered variable influences the adsorption uptake (%). Fig. 6 revealed a line that separates the significant effects from those that were not. The confidence interval chosen was 95%. All variables and interactions with an effect below the limit of significance (95% confidence interval) namely, variable4 (T), and all products containing this variable (interactions containing temperature), as well as the interaction pH × S/L × C_0 were disregarded and not represented in the model. The

Table 7 Estimation of the significant of effects using Student's t-test

Terms	Effect	Estimate	Error standard	Value of t_i	Value of p	Significant
Constante		23.8962	0.3005	79.5099	0.0080	Significant
pH	−28.4656	−14.2328	0.3005	−47.3568	0.0134	Significant
r (s/l)	31.8075	15.9038	0.3005	52.9167	0.0120	Significant
C_0	−7.9101	−3.9551	0.3005	−13.1597	0.0483	Significant
T	−3.7464	−1.8732	0.3005	−6.2328	0.1013	Not significant
pH × r (s/l)	−25.6274	−12.8137	0.3005	−42.6351	0.0149	Significant
pH × C_0	−8.7402	−4.3701	0.3005	−14.5407	0.0437	Significant
pH × T	1.6877	0.8438	0.3005	2.8077	0.2178	Not significant
r (s/l) × C_0	−10.1716	−5.0858	0.3005	−16.9220	0.0376	Significant
r (s/l) × T	−2.3732	−1.1866	0.3005	−3.9481	0.1579	Not significant
C_0 × T	1.3479	0.6739	0.3005	2.2424	0.2670	Not significant
pH × r (s/l) × C_0	6.5570	3.2785	0.3005	10.9085	0.0582	Not significant
pH × r (s/l) × T	1.3278	0.6639	0.3005	2.2090	0.2706	Not significant
pH × C_0 × T	0.1564	0.0782	0.3005	0.2602	0.8380	Not significant
r (s/l) × C_0 × T	1.2010	0.6005	0.3005	1.9980	0.2954	Not significant

Table 8 Analysis of variance (ANOVA) for the adsorption of MB onto the NaX zeolite

Source	ddl	Sum of squares	Mean square	F-Value	p-Value
Model	14	11 167.0081	797.6434	551.9165	0.0334
Linear	4	7594.4591	1898.6148	1313.7160	0.0207
pH	1	3241.1587	3241.1587	2242.6676	0.0134
r (s/l)	1	4046.8778	4046.8778	2800.1720	0.0120
C_0	1	250.2795	250.2795	173.1769	0.0483
T	1	56.1432	56.1432	38.8474	0.1013
2-Factor interactions	6	3387.6547	564.6091	390.6722	0.0387
pH × r (s/l)	1	2627.0571	2627.0571	1817.7499	0.0149
pH × C_0	1	305.5653	305.5653	211.4310	0.0437
pH × T	1	11.3928	11.3928	7.8831	0.2178
r (s/l) × C_0	1	413.8448	413.8448	286.3532	0.0376
r (s/l) × T	1	22.5276	22.5276	15.5876	0.1579
C_0 × T	1	7.2672	7.2672	5.0284	0.2670
3-Factor interactions	4	184.8942	46.2235	31.9836	0.1318
pH × r (s/l) × C_0	1	171.9750	171.9750	118.9954	0.0582
pH × r (s/l) × T	1	7.0521	7.0521	4.8796	0.2706
pH × C_0 × T	1	0.0978	0.0978	0.0677	0.8380
r (s/l) × C_0 × T	1	5.7692	5.7692	3.9919	0.2954
Error	1	1.4452	1.4452		
Total	15	11 168.4533			

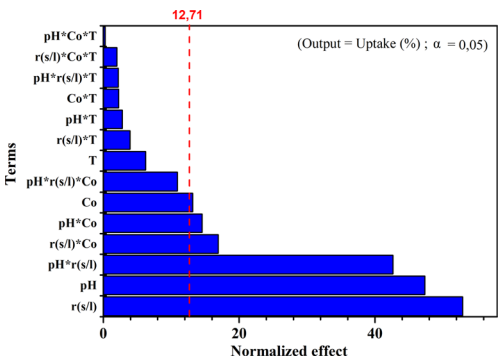

Fig. 6 Pareto chart for MB adsorption on NaX zeolite.

corresponding Pareto chart shows that the coefficient of determination was approximately (R^2 = 91.43%), which was highly satisfactory. The most dominant factor was S/L followed by pH.

5. Conclusions

In this study, the hydrothermal synthesis of NaX zeolite was successfully carried out at 100 °C, 24 h and under autogenous pressure. The high frequency bands at 3650 cm^{-1} of hydroxyl groups (O–H), which facilitates MB adsorption, were highlighted during FTIR analysis. The observed high specific surface area (375 m^2 g^{-1}) and micropore volume (0.12 cm^3 g^{-1}) of the synthesized NaX facilitate its usage in the adsorption of organic molecules. The isotherm modelling study showed that MB adsorption onto NaX followed Langmuir isotherm based on the results of error functions R^2, Adj. R^2, RSS, MSE, χ^2, RMSE and AIC and AICc criteria, while kinetic modelling results revealed the fitting of PSO kinetic model at low MB concentrations (5–30 mg L^{-1}) and PFO kinetic model at high concentrations (50–120 mg L^{-1}). However, the adsorption kinetic data followed PSO kinetic model at varying temperature, suggesting a rate limiting

step and a chemisorption process. The thermodynamic study reveals that MB adsorption NaX was a spontaneous and an exothermic process. Using a full 2-level factorial design, we were able to identify the optimum conditions for the adsorption of MB onto NaX accurately and efficiently, minimising the number of trials required. The estimation study of the significant effects using Student's *t*-test revealed that the temperature was not significant, and the other interactions were significant. The regression equation with 16 factors was simplified to only 7. The resulting model was validated by an analysis of variance (ANOVA) confirming its relevance. Finally, the Pareto chart showed that the coefficient of determination ($R^2 = 91.43\%$) was highly satisfactory and the most influent variable in the adsorption of MB onto the NaX zeolite was S/L followed by pH.

Data availability

The data supporting this article have been included as a part of ESI.†

Conflicts of interest

There are no conflicts to declare.

Acknowledgements

Moonis Ali Khan acknowledges the financial support through Researchers Supporting Project number (RSP2024R345), King Saud University, Riyadh. Saudi Arabia.

References

1 A. Aid, S. Amokrane, D. Nibou, E. Mekatel, M. Trari and V. Hulea, *Water Sci. Technol.*, 2018, **77**, 60–69, DOI: **10.2166/wst.2017.509**.
2 S. F. Azha, M. Shahadat and S. Ismail, *Dyes Pigm.*, 2017, **145**, 550–560, DOI: **10.1016/j.dyepig.2017.05.009**.
3 F. Kooli, Y. Liu, R. Al-Faze and A. AlSuhaimi, *Appl. Clay Sci.*, 2015, **116**, 23–30, DOI: **10.1016/j.clay.2015.07.044**.
4 S. K. Pradhan, V. Pareek, J. Panwar and S. Gupta, *J. Water Process Eng.*, 2019, **32**, 100917, DOI: **10.1016/j.jwpe.2019.100917**.
5 E. H. Mekatel, S. Amokrane, A. Aid, D. Nibou and M. Trari, *C. R. Chim.*, 2015, **18**(3), 336–344, DOI: **10.1016/j.crci.2014.09.009**.
6 I. A. W. Tan, A. L. Ahmad and B. H. Hameed, *Desalination*, 2018, **225**, 13–28, DOI: **10.1016/j.desal.2007.07.005**.
7 R. I. Foster, J. T. Amphlett, K. W. Kim, T. Kerry, K. Lee and C. A. Sharrad, *J. Ind. Eng. Chem.*, 2020, **81**, 144–152, DOI: **10.1016/j.jiec.2019.09.001**.
8 A. Kornilov, E. Piterkina, K. Shcherbakova, A. Makarov and O. Dmitrieva, *Radiochemistry*, 2020, **62**(2), 173–176, DOI: **10.1134/S1066362220020046**.
9 M. Hoyer, D. Zabelt, R. Steudtner, V. Brendler, R. Haseneder and J.-U. Repke, *Sep. Purif. Technol.*, 2014, **132**, 413–421, DOI: **10.1016/j.seppur.2014.05.044**.
10 A. Akbari, J. Remigy and P. Aptel, *Chem. Eng. Process.*, 2002, **41**(7), 601–609, DOI: **10.1016/S0255-2701(01)00181-7**.
11 H. Mekatel, S. Amokrane, B. Bellal, M. Trari and D. Nibou, *Chem. Eng. J.*, 2012, **200**, 611–618, DOI: **10.1016/j.cej.2012.06.121**.
12 X. Yang, Z. Zhang, S. Kuang, H. Wei, Y. Li, G. Wu, A. Geng, Y. Li and W. Liao, *Hydrometallurgy*, 2020, **194**, 105343, DOI: **10.1016/j.hydromet.2020.105343**.
13 M. Goleij and H. Fakhraee, *Iran. J. Chem. Chem. Eng.*, 2017, **36**(5), 129–141, DOI: **10.30492/IJCCE.2017.25481**.
14 S. Poorsadeghi, M. Z. Kassaee, H. Fakhri and M. Mirabedini, *Iran. J. Chem. Chem. Eng.*, 2017, **36**(4), 91–99, DOI: **10.30492/IJCCE.2017.28714**.
15 M. A. Khan, A. A. Alqadami, S. M. Wabaidur and B. H. Jeon, *Nanomaterials*, 2023, **13**(7), 1193, DOI: **10.3390/nano13071193**.
16 A. A. Alqadami, S. M. Wabaidur, B. H. Jeon and M. A. Khan, *Biomass Convers. Biorefin.*, 2023, 1–12, DOI: **10.1007/s13399-022-03711-7**.
17 H. Majdoubi, A. A. Alqadami, R. E. K. Billah, M. Otero, B. H. Jeon, H. Hannache, Y. Tamraoui and M. A. Khan, *Int. J. Environ. Res. Public Health*, 2023, **20**(1), 831, DOI: **10.3390/ijerph20010831**.
18 S. M. Wabaidur, M. A. Khan, M. R. Siddiqui, M. Otero, B. H. Jeon, Z. A. Alothman and A. A. H. Hakami, *J. Mol. Liq.*, 2020, **317**, 113916, DOI: **10.1016/j.molliq.2020.113916**.
19 E. T. Wahyuni, D. Rendo and S. Suherman, *Global NEST J.*, 2021, **23**, 119–126, DOI: **10.30955/gnj.003249**.
20 M. Andrunik, M. Skalny, M. Gajewska, M. Marzec and T. Bajda, *Heliyon*, 2023, **9**(10), E20572, DOI: **10.1016/j.heliyon.2023.e20572**.
21 S. Amokrane, R. Rebiai and D. Nibou, *J. Appl. Sci.*, 2007, **7**, 1985–1988, DOI: **10.3923/jas.2007.1985.1988**.
22 M. Senila and C. Oana, *Heliyon*, 2024, **10**(3), E25303, DOI: **10.1016/j.heliyon.2024.e25303**.
23 D. Nibou and S. Amokrane, *J. Mol. Liq.*, 2021, **323**, 114642, DOI: **10.1016/j.molliq.2020.114642**.
24 G. Engelhardt, *Introduction to Zeolite Science and Practice*, ed. H. VanBekkum, E. M. Flanigen and J. C. Jansen, Elsevier Amesterdam, 1991.
25 E. H. Zouaoui, N. Djamel, W. A. Wan Ab Karim Ghani and A. Samira, *Iran. J. Chem. Chem. Eng.*, 2021, **40**(4), 1195–1215, DOI: **10.30492/IJCCE.2020.40342**.
26 A. Dyer, *An Introduction to Zeolite Molecular Sieve*, John Wiley, London, 1988.
27 D. W. Breck, *ZeoliteMolecularsieves-Structure Chemistry and Use*, WileyInterscience, New York, 1974.
28 C. Baerlicher, W. M. Meier and D. H. Olson, *Atlas of Zeolite Framework Types*, Elsevier, Amesterdam, 5th revised edn, 2001.
29 Q. F. Lin, Z. R. Gao, C. Lin, S. Zhang, J. Chen, Z. Li, X. Liu, W. Fan, J. Li, X. Chen, M. A. Camblor and F. J. Chen, *Science*, 2021, **374**(6575), 1605–1608, DOI: **10.1126/science.abk3258**.
30 J. Li, Z. R. Gao, Q. F. Lin, C. Liu, F. Gao, C. Lin, S. Zhang, H. Deng, A. Mayoral, W. Fan, S. Luo, X. Chen, H. He,

M. A. Camblor, F. J. Chen and J. Yu, *Science*, 2023, **379**(6629), 283–287, DOI: **10.1126/science.ade1771**.

31 Z. R. Gao, H. Yu, F. J. Chen, A. Mayoral, Z. Niu, Z. Niu, X. Li, H. Deng, C. Márquez-Álvarez, H. He, S. Xu, Y. Zhou, J. Xu, H. Xu, W. Fan, S. R. G. Balestra, C. Ma, J. Hao, J. Li, P. Wu, J. Yu and M. A. Camblor, *Nature*, 2024, **628**(8006), 99–103, DOI: **10.1038/s41586-024-07194-6**.

32 N. Y. Baouali, D. Nibou and S. Amokrane, *Iran. J. Chem. Chem. Eng.*, 2022, **41**(6), 1907–1920, DOI: **10.30492/IJCCE.2021.128624.4168**.

33 S. Sivalingam and S. Sen, *Appl. Surf. Sci.*, 2019, **463**, 190–196, DOI: **10.1016/j.apsusc.2018.08.019**.

34 Y.-P. Zhao, D.-X. Guo, S.-F. Li, J.-P. Cao and X.-Y. Wei, *Desalin. Water Treat.*, 2020, **185**, 355–363, DOI: **10.5004/dwt.2020.25424**.

35 D. Nibou, H. Mekatel, S. Amokrane, M. Barkat and M. Trari, *J. Hazard. Mater.*, 2010, **173**(1–3), 637–646, DOI: **10.1016/j.jhazmat.2009.08.132**.

36 R. S. AbdElkader, M. K. Mohamed, Y. A. Hasanien and E. M. Kandeel, *J. Cluster Sci.*, 2023, **34**, 3147–3163, DOI: **10.1007/s10876-023-02454-3**.

37 M. Barkat, D. Nibou, S. Chegrouche and A. Mellah, *Chem. Eng. Process. Process Intensif.*, 2009, **48**(1), 38–47, DOI: **10.1016/j.cep.2007.10.004**.

38 M. M. J. Treacy and J. B. Hugging, *Collection of Simulated X Patterns for Zeolites*, Elsevier, 4th revised edn, 2001.

39 S. K. Masoudian, S. Sadighi and A. Abbasi, *Bull. Chem. React. Eng. Catal.*, 2013, **8**(1), 54–60, DOI: **10.9767/bcrec.8.1.4321.54-60**.

40 D. Ferhat, D. Nibou, E. Mekatel and S. Amokrane, *Iran. J. Chem. Chem. Eng.*, 2019, **38**(6), 63–81, DOI: **10.30492/ijcce.2019.33252**.

41 D. Nibou, S. Khemaissia, S. Amokrane, M. Barkat, S. Chegrouche and A. Mellah, *Chem. Eng. J.*, 2011, **172**(1), 296–305, DOI: **10.1016/j.cej.2011.05.113**.

42 Y. Kuang, X. Zhang and S. Zhou, *Water*, 2020, **12**(2), 587, DOI: **10.3390/w12020587**.

43 M. T. Yagub, T. K. Sen and H. M. Ang, *Water, Air, Soil Pollut.*, 2012, **223**, 5267–5282, DOI: **10.1007/s11270-012-1277-3**.

44 M. T. Yagub, T. K. Sen, S. Afroze and H. M. Ang, *Adv. Colloid Interface Sci.*, 2014, **209**, 172–184, DOI: **10.1016/j.cis.2014.04.002**.

45 B. K. Nandi, A. Goswami and M. K. Purkait, *J. Hazard. Mater.*, 2009, **161**(1), 387–395, DOI: **10.1016/j.jhazmat.2008.03.110**.

46 B. K. Nandi, A. Goswami and M. K. Purkait, *Appl. Clay Sci.*, 2009, **42**(3–4), 583–590, DOI: **10.1016/j.clay.2008.03.015**.

47 N. Hajnajafi, A. Khorshidi, A. G. Gilani and F. Verpoort, *Removal of Methylene Blue from Aqueous Solution by Polydopamine@ Zeolitic Imidazolate-67*, 2021, DOI: **10.21203/rs.3.rs-1162284/v1**.

48 Y. Dehmani, B. B. Mohammed, R. Oukhrib, A. Dehbi, T. Lamhasni, Y. Brahmi, A. El-Kordy, D. S. Franco, J. Georgin, E. C. Lima and A. A. Alrashdi, *Arabian J. Chem.*, 2024, **17**(1), 105474, DOI: **10.1016/j.arabjc.2023.105474**.

49 M. A. M. Lawrence, R. K. Kukkadapu and S. A. Boyd, *Appl. Clay Sci.*, 1998, **13**, 13–20, DOI: **10.1016/S0169-1317(98)00009-X**.

50 A. Gürses, Ç. Doğar, M. Yalçın, M. Açıkyıldız, R. Bayrak and S. Karaca, *J. Hazard. Mater.*, 2006, **131**(1–3), 217–228, DOI: **10.1016/j.jhazmat.2005.09.036**.

51 D. Nibou, S. Amokrane, H. Mekatel and N. Lebaili, *Phys. Procedia*, 2009, **2**, 1433–1440, DOI: **10.1016/j.phpro.2009.11.113**.

52 S. Bentahar, A. Dbik, M. El Khomri, N. El Messaoudi and A. Lacherai, *J. Environ. Eng.*, 2017, **5**(6), 5921–5932, DOI: **10.1016/j.jece.2017.11.003**.

53 I. Langmuir, *J. Am. Chem. Soc.*, 1916, **38**(11), 2221–2295, DOI: **10.1021/ja02268a002**.

54 H. Freundlich, *Z. Phys. Chem.*, 1907, **57**(1), 385–470, DOI: **10.1515/zpch-1907-5723**.

55 M. I. Temkin, *Zh. Fiz. Khim.*, 1941, **15**, 296–332.

56 S. Y. Elovich, O. G. Larinov, I. Akad, N. SSSR and O. Khim, *Nauk*, 1962, **2**(2), 209–216.

57 A. Benmessaoud, D. Nibou, E. H. Mekatel and S. Amokrane, *Iran. J. Chem. Chem. Eng.*, 2020, **39**(4), 153–171, DOI: **10.30492/ijcce.2019.35116**.

58 H. Xi, Z. Li, H. Zhang, X. Li and X. Hu, *Sep. Purif. Technol.*, 2003, **31**, 41–45, DOI: **10.1016/S1383-5866(02)00150-8**.

59 N. Dahdouh, S. Amokrane, R. Murillo, E. Mekatel and D. Nibou, *J. Polym. Environ.*, 2020, **28**, 271–283, DOI: **10.1007/s10924-019-01605-w**.

60 E. Mekatel, S. Amokrane, M. Trari, D. Nibou, N. Dahdouh and S. Ladjali, *Arabian J. Sci. Eng.*, 2019, **44**(6), 5311–5322, DOI: **10.1007/s13369-018-3575-6**.